A MICROGRAVITY ISOLATION MOUNT

D. I. Jones, A. R. Owens, R. G. Owen, G. Roberts, *
D. W. Wyn-Roberts & A. A. Robinson. **

ABSTRACT

In this paper we discuss the design and preliminary testing of a system for isolating microgravity sensitive payloads from spacecraft vibrational and impulsive disturbances. The Microgravity Isolation Mount (MGIM) concept consists of a platform which floats almost freely within a limited volume inside the spacecraft, but which is constrained to follow the spacecraft in the long term by means of very weak springs. The springs are realised magnetically and form part of a six degree of freedom active magnetic suspension system. The latter operates without any physical contact between the spacecraft and the platform itself. Power and data transfer is also performed by contactless means. Specifications are given for the expected level of input disturbances and the tolerable level of platform acceleration. The structural configuration of the mount is discussed and the design of the principal elements, i.e. actuators, sensors, control loops and power/data transfer devices are described. Finally we describe the construction of a hardware model that is being used to verify the predicted performance of the MGIM.

INTRODUCTION

It has long been proposed that the microgravity environment of Earth orbit has advantages for experimental work in the fields of fluid science, organic and inorganic materials preparation and the life sciences. Wilhelm [1] reviews some of the preliminary work which has already been performed in materials processing. If space manufacture is to achieve commercial viability then further research is required now to establish suitable processing techniques which take full advantage of the unique on-orbit environment. It has been established [2] that many of the proposed processing techniques are critically dependent upon achieving lower levels of microacceleration than exist in current spacecraft. The experience gained in Europe on Spacelab will be applied to achieving a low level microgravity environment for experimenters on the Columbus programme in cooperation with the U.S. Space Station.

The factors which determine the microgravity environment have been identified [3] and may be classified by frequency range as follows:

1) quasi-static, external disturbances due to aerodynamic drag and gravity gradient effects.

---

* University College of North Wales, Bangor, Great Britain.
** European Space Technology Center, Noordwijk, The Netherlands.

2) Low frequency vibration sources, e.g. responses of large flexible elements (solar arrays, antennae), crew motion, spacecraft attitude control, robotic manipulators.

3) Medium/high frequency vibration caused by on-board equipment (motors, pumps etc.)

Disturbances in class 1 are minimised by careful consideration of spacecraft orbital altitude and mass distribution; generally it is thought that a quasi-static level of the order of 1μg is achievable. Lower values may be possible by reducing the effects of aerodynamic drag by active acceleration control using thrust compensation.

Isolation of the experimental payload from class 3 disturbances is relatively straightforward and a passive, mechanical suspension would probably suffice since the microgravity requirement is less stringent in this range.

In many ways, the most difficult disturbances to deal with are those in class 2. The concept of a Man-Tended Free Flyer (MTFF) is currently being investigated by ESA as part of its Columbus programme. Here, microgravity payloads requiring infrequent crew attention are placed aboard an autonomous, unmanned free flyer. This offers extended periods free from the disturbances associated with the Space Station, the Flyer returning periodically to the Space Station for servicing. Vibration due to on-board equipment may still be a problem. The difficulty of access, if human intervention is required, is also a drawback.

In the case of the Columbus attached Pressurised Module (PM), additional disturbances occur due to the continual presence of men and due to vibrations transmitted from the Space Station itself. Therefore, especially the PM but also quite possibly the MTFF require a suspension mechanism which isolates payloads from class 2 and class 3 disturbances but which is controlled to maintain a long-term position adjacent to its supporting frame. Here we propose a Microgravity Isolation Mount (MGIM) for this purpose.

The MGIM consists of support frame and a platform for mounting the experiment. Frame and platform are separated by actively controlled isolators.

In this paper we discuss what levels of acceleration are allowable on the platform and what levels are present on the supporting frame. A design proposal for the MGIM is then presented and its component parts discussed. Finally, we assess the potential performance of the MGIM and give experimental results from a preliminary rig which has been constructed to verify actual operational capabilities.

REQUIRED ACCELERATION LEVELS.

Studies of the microacceleration levels required for successful experimentation have shown that the class 2 frequency band is critical. Curve (a) in Fig.1 shows a sinusoidal specification of acceptable acceleration levels, based on the envelope of several curves given by Tiby & Langbein [5]. Their curves were derived from theoretical models which indicate that the allowed acceleration exhibits a constant limit at low frequencies and a square law dependency at high frequencies. Curve (b) is the design specification for Eureca [6] while curve (c) is the proposed specification for the U.S. Space Station [7]. Taking into account each of these curves, we formulated Fig.2a as an appropriate specification for our work. Below 1.5 Hz a constant level of 10^{-5}g is specified as the minimum to be achieved while between 1.5 Hz and 15 Hz an f^2 variation, compatible with Fig.1a, is assumed. Above 15 Hz a 10^{-3}g upper limit is imposed in consideration of practical constraints such as damage to delicate instrumentation. A supplementary (dotted) curve in Fig.2a continues the f^2 variation down to the 10^{-6}g level and represents the ultimate objective of our work.

Our guideline sinusoidal characteristic for the translational vibration of the supporting frame is shown in Fig.2b. In practice this vibration characteristic will be produced by several different sources, such as spacecraft subsystems (pumps, steerable antennae etc.), crew motion and thrusters which will interact on the nonlinear dynamic components of the spacecraft structure. The result will be a random combination of impulsive and periodic signals with broadband "noise" as a base and probably containing spectral peaks related to the natural modes of the spacecraft structure. Since modelling of such a complex system is a considerable task in itself, and in view of the paucity of measured data (especially in the lower frequency range), Fig.2b was adopted as an envelope which encompasses all these effects. An f^2 variation is assumed below 3 Hz and a constant limit of 10^{-1}g above 3 Hz. In fact, comparison with known characteristics for other transportation systems [4] shows it to be a worst case since it exceeds considerably the expected on-orbit vibration environment. This is supported by [2] where the measured acceleration data presented for the D-1 mission rarely reaches 10^{-2}g except during orbit trim burns.

Combining figures 2a and 2b gives the transmissibility function, Fig.2c which shows that below 0.03 Hz it is permissible for the platform to follow the outer frame and this defines the break frequency required of the MGIM. This corresponds to a maximum amplitude of approximately 4 mm which is an important parameter in designing the MGIM actuators. Above this frequency at least a -40dB/decade roll-off is required, up to 1.5 Hz, to maintain the platform acceleration at or below 10^{-5}g.

STRUCTURAL DESIGN

Our preliminary design study is based on the structural concept shown in Fig.3 where the payload is affixed to a central platform. The platform is to be controlled in six degrees of freedom so that it remains at a cen-

tral position within its supporting frame. For the purposes of the present study, it has been assumed that the unit fits into a cube of about 1 m side and has a maximum mass of approximately 200 kg, but this does not mean that other configurations cannot be accommodated. Both platform and supporting frame should be as rigid as possible and the platform should be well-damped so that any high frequency modes will decay quickly. In conflict with this, low platform weight is desirable so that payload mass is maximised. This can be achieved with a platform having a closed-cell honeycomb internal structure with a stainless steel surface skin. The central platform allows easy access to the payload and is adaptable to various sizes and shapes of experiment modules. A locking mechanism is provided which clamps the platform securely for periods of launch and manoeuvre.

Modules containing actuators and sensors are situated at each corner, the actuators acting together to control translational motion and differentially to control rotational motion. With this configuration the actuators act directly on the platform and a modular construction facilitates assembly.

Any combination of platform and payload will have an uneven mass distribution and estimates were made of the following parameters:

i) the total mass of the platform and payload,

ii) the position of the centre of mass relative to the geometric centre,

iii) the moments of inertia about the principal axes,

iv) the orientation of the principal axes relative to the reference axes.

For simplicity, the analysis was confined to a two dimensional representation with the geometric centre taken as the origin.

Figures 4 and 5 show how the five parameters vary as payload asymmetry increases.

In a case thought to be typical of a platform/payload combination, Fig.4 shows a heavier experiment on the right hand side having drawn the centre of mass up and across to the right. The total platform mass is 95 kg with the centre of mass pulled 9 cm radially away from the origin. The principal axes are only rotated by about 9°.

In the previous case, platform and payload are assumed to have a uniform density of 320 kg/m^3 but in Fig.5 the shaded area represents a solid block of aluminium. This probably represents an extreme case of asymmetry. The total mass is now 150 kg with the radius of the centre of mass pulled to 20 cm from the origin and the principal axes rotated by 14°.

More accurate computation of these parameters is desirable but two tentative conclusions may be drawn from these results:

i) Insisting that experiment packages be configured such that they conform to a 10 cm envelope for centre of mass displacement does not place unreasonable constraints on mass asymmetry,

ii) The moment on the platform, due to the line of action of the actuators not being through the centre of mass, will induce angular motion (and amplification of linear acceleration at the periphery). By far the major contributor to this moment is the translation of the centre of mass; orientation of the principal axes is relatively unimportant.

ELECTRICAL POWER, COOLING AND DATA TRANSMISSION.

The connections between platform and supporting frame must perform three separate functions:

i) supply of electrical power to the platform,

ii) transport of cooling fluid to and from the platform,

iii) transmission of control and data signals.

Any physical connection will form a compliant element between the frame and platform thus introducing direct transmission of vibration. It is therefore crucial to investigate to what extent these functions can be performed without recourse to a direct umbilical link.

Electrical power transmission may be substantial for some experiments such as crystal growth from a melt in a furnace. We have assumed a load rating of 1 kW and investigated the use of a transformer with loose-coupled secondary to effect power transmission. Fig.6 shows that the primary winding is wound onto the core of the transformer in the usual manner, but the secondary winding has a 7 mm clearance in all directions between the core and former. A prototype of this transformer has been constructed, the primary winding being driven with a square wave derived from a 150 V d.c. supply by a MOS transistor bridge. The secondary is connected directly to a bridge rectifier and smoothing capacitor with resistive load. Power transfer of 1 kW with good regulation properties has been successfully achieved [8].

Cooling the payload is the most difficult task. Applying the Stefan-Boltzmann law of radiation shows that for the 6 m^2 suface area of our unit, a surface temperature of 46°C. results from dissipating 1 kW with an ambient temperature of 20°C. It is likely that these figures represent a pessimistic case and could be improved upon by:

i) placing one of the MGIM walls adjacent to the spacecraft outer skin to take advantage of a reduced ambient temperature,

ii) changing the MGIM shape from a cube to "flatter" proportions giving an improved ratio of surface area to volume,

iii) reducing the input power needed to maintain furnace temperature by means of improved thermal insulation.

For greater power levels, forced liquid cooling is the only realistic method requiring flexible tubing between frame and platform. For the specification given previously, the limit of stiffness for this tubing is of the order of 2-3 N/m and careful dynamic characterisation would be required when designing such an umbilical. It is worth stating that the thermal problem exists whatever method of vibration isolation is being considered.

The non-contact transmission of data presents little problem and we have demonstrated an infra-red optical link operating at over 100 kbit/s- more than adequate for the expected 100 Hz sampling rate. A source/receiver distance of 30 mm and lateral movement up to a radius of about 30 mm can be tolerated even in the presence of fairly high levels of ambient light.

Clearly, there is an advantage from the point of view of vibration isolation in operating the MGIM as a wholly non-contact system. The preceding discussion indicates that it is also feasible to maintain platform services in such a way and so we proceed to discuss how non-contact vibration control may be achieved.

ACTUATORS AND SENSORS.

The sensors referred to in Fig.3 are non-contact devices. There are eight sensors sited to measure platform displacement relative to the outer frame. They operate as differential capacitance bridges detecting the movement of a central plate affixed to the platform, as shown in Fig.7. Stray capacitances from the sensing plates and connecting leads to ground, and between the primary and secondary windings of the transformer, are eliminated by guard techniques. Conventional phase sensitive detection yields a linear d.c. output which is independent of the dielectric constant of the gap and, by making the central plate much larger than the two sensor plates, is sensitive to motion in one axis only.

The actuators must also be non-contact devices; they are effectively small linear motors as shown in detail in Fig.8. Rare earth permanent magnets establish a flux density in the bore of the stator. A thin, planar armature inserted into the bore produces force on the platform in one direction while allowing free movement along the other two directions to the limits of the bore gap. It has been estimated [4] that each actuator must provide approximately 0.01 N of force. The actuator shown in Fig.8 has a 72 conductor armature and a stator bore flux density of 0.14 T.

Fig.9 is its measured characteristic showing that a force of 0.01 N is achieved with about 30 mA of armature current. Evidently, the power requirements are very low and the actuator does not appear to be a limiting factor in this application.

CONTROL TECHNIQUES.

A one degree of freedom analysis shows that, for the case of a low umbilical stiffness, acceptable system performance can be obtained in a straightforward manner using platform position sensing only. The block diagram of the control loop for one axis is shown in Fig.10. Its transfer function is given by:

$$\frac{y}{x} = \frac{s + \gamma}{s^3 + \alpha s^2 + s + \gamma}$$

where the parameters α and γ are related to the chosen natural fequency, the system mass and specified control loop gains by the following substitutions:

$\omega_o^2 = C/M$ where: ω_o = system natural frequency

$\alpha\omega_o = a$ a,b = lead-lag time constants

$\gamma\omega_o = bC$ M = platform + payload mass

C = feedback loop gain

Assuming that $\alpha / \gamma = 30$, computer simulation has shown [8] that the frequency response of equation (1) agrees well with the requirement of Fig.2.

In order to assess system performance in the case where the centre of mass is not coincident with the platform's geometric centre, a two degree of freedom model was simulated - see Fig.11. Here the platform is in plan view and is controlled by two actuators at either corner exerting forces F_1 and F_2. Sensors at these points measure the gaps x_1 and x_2. Linear motion is confined to the x direction. The moments are given by $F_1 l_a$ and $F_2 l_b$, respectively, and induce an angular displacement, θ, about the z axis. The control loops for the actuators are as shown in Fig.10 and are independent; no control loop is implemented for explicit control of rotation.

Fig.12 shows the step response of the two platform ends, assuming a 7 cm displacement of the centre of mass in the y direction. Curves a and b show that the overshoot of the two ends are different due to the asymmetry but still exhibit acceptable damping. Curve c shows the response of the centre of mass for comparison. The peak angle induced is shown in Fig.13 to be limited to an acceptable value of 0.26 milli-radians. Fig.14 shows

the variation of the peak angle for greater displacements of the centre of mass. This preliminary simulation indicates that rotational effects do not compromise the MGIM performance and we now intend to investigate this further with a six degree of freedom model for various actuator/sensor configurations.

EXPERIMENTAL VERIFICATION

In order to obtain experimental verification of the performance of our proposed design we have constructed two test rigs where the platform is supported on an air bed giving very low values of friction.

The first test rig consists of two parallel air tracks holding a platform of approximately 8.5 kg weight and giving 5.5 mm of free movement as shown in Fig.15. Actuators and position sensors, similar to those described previously, are used to control the platform motion. The digital compensator is designed for 0.5 Hz bandwidth and incorporates integral control since it is necessary to counteract the disturbance forces from the air jet system and any levelling mis-alignment of the air track.

Fig.16 shows the sinusoidal acceleration frequency response of the platform to an imposed vibration of the supporting frame. It does not quite conform with the expected frequency response (dotted line), due to the resonant peak at 0.5 Hz. Nevertheless, it is quite clear that the rig is isolating the platform successfully from high frequency vibration while maintaining its position adjacent to the supporting frame at low frequency.

This result encouraged us to construct a second test rig which has a heavier platform and extends control to three degrees of freedom. In order to avoid the imperfections associated with the first rig, this second rig was built to a higher standard so that a lower bandwidth controller could be employed and allowing testing of our non-contact "umbilical" technology.

The rig consists of a heavy slate plinth and surface plate on which are mounted four air pads - see Fig.17. These support a 35 kg platform of honeycomb construction, giving free motion in the horizontal plane. Surrounding the platform is an outer frame which is free to move in one axis and is driven by a vibrator. The actuators and position sensors are mounted between the platform and outer frame and allow $\pm$ 5 mm of movement in each horizontal axis. As shown in Fig.18, power supply to the on-board electronics is by means of auxiliary secondaries on the loosely coupled transformer to give 5V and $\pm$ 12V d.c. A servo-accelerometer (Sundstrand QA 1400) is mounted at the platform extremity to measure acceleration in either the x or y axes. Data from this is passed via a programmable analog anti-alias filter (under control of the on-board computer) before being sampled at 100 Hz and digitised with 12 bit resolution. This data is then passed back to external instrumentation via the optical data link. A further two-way optical link allows external control of the on-board FORTH computer, which is responsible for data acquisition, as well as switching a 1 kW dummy load.

The digital lead/lag compensators are implemented for the three channels (x, y, θ) on an MC6809 microprocessor sampling at 100 Hz. Controller outputs are applied to the actuator coils by power operational amplifiers.

As well as its performance in vibration isolation, this rig will allow us to test the effects of:

i) centre of mass displacement,

ii) transformer power level changes producing disturbance forces on the platform,

iii) other actuator/sensor configurations,

iv) other control strategies,

v) the acceleration spectrum with a stochastic vibration input.

CONCLUSIONS.

To date our study has concentrated on formulating a design concept for the MGIM. In this paper we have discussed the required performance specification and outlined the mechanical structure and the design of functional components of an MGIM capable of achieving this.

The one degree of freedom test rig has largely confirmed the potential of our design. We now intend to concentrate on using the three degree of freedom test rig to demonstrate further the MGIM technology outlined here. In conjunction we are preparing a six degree of freedom computer model of the MGIM in order to design multivariable control laws and assess the impact of offset centre of mass on system performance.

REFERENCES.

[1] Wilhelm, J.P.
"Industrial Research Opportunities in Space".
IEEE EASCON '84, 17th Annual Electronics & Aerospace Conf.,
Sept. 10-12, 1984.

[2] Hamacher, H., Merbold, U. & Jilg, R.
"The Microgravity Environment of the D-1 Mission".
Proc. 37th IAF Conference, Innsbruck, 1986. Paper IAF-86-268.

[3] Olsen, R.E. & Mockovciak, J.
"Operational Factors Affecting Microgravity Levels in Orbit".
Jour. Spacecraft, Vol. 18, 2, 1981, pp. 141-144.

[4] Jones, D.I., Owens, A.R. & Owen, R.G.
"Microgravity Isolation Mount: Design Report".
Report of a study performed under ESTEC contract No. 6380/85 by U.C.N.W., Bangor.

[5] Tiby, C. & Langbein, D.
"Allowable g-levels for Microgravity Payloads".
Report of a study performed under ESTEC contract No. 5504/83 by Battelle Institute, Frankfurt.

[6] Eilers, D.
"Microgravity Conditions for Orbiting Platforms".
Annual DGLR Conference, Germany, 1983.

[7] Teledyne Brown Engineering
"Low Acceleration Characterization of Space Station Environment".
Report prepared for N.A.S.A., Marshall Space Flight Center, Oct. 1985.

[8] Jones, D.I., Owens, A.R. & Owen, R.G.
"A Microgravity Isolation Mount".
Proc. 37th IAF Conference, Innsbruck, 1986. Paper IAF-86-270.

ACKNOWLEDGEMENTS.

The work presented here was performed as part of ESTEC contract No. 6380/85/NL/AN.

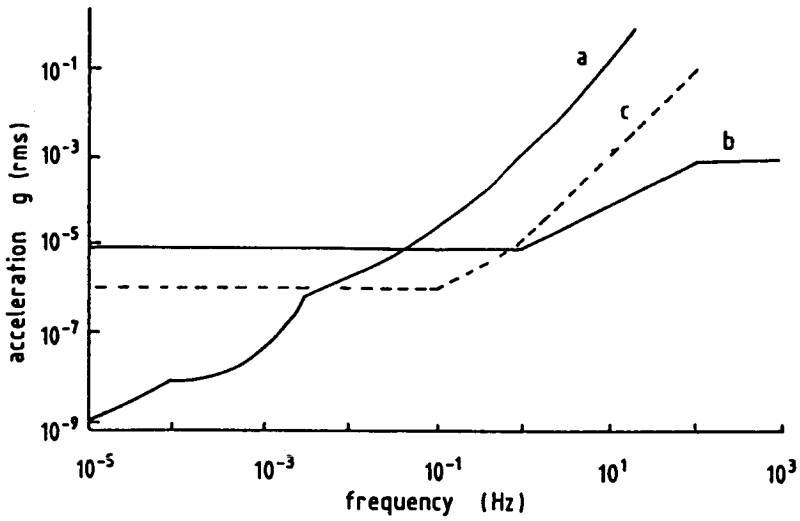

Key

a) envelope of Battelle output level

b) EURECA

c) U. S. space station usable specification

Fig.1 Relationship between sinusoidal specifications.

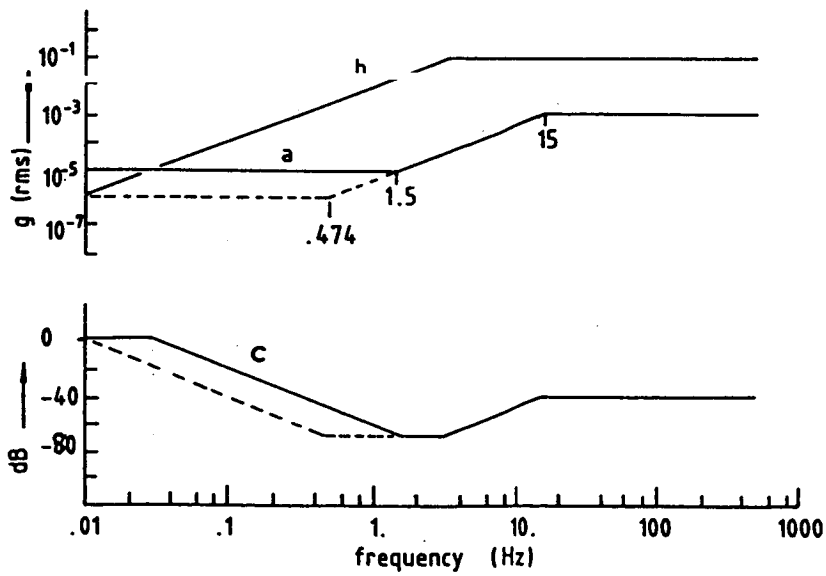

Fig.2 Assumed sinusoidal specification.

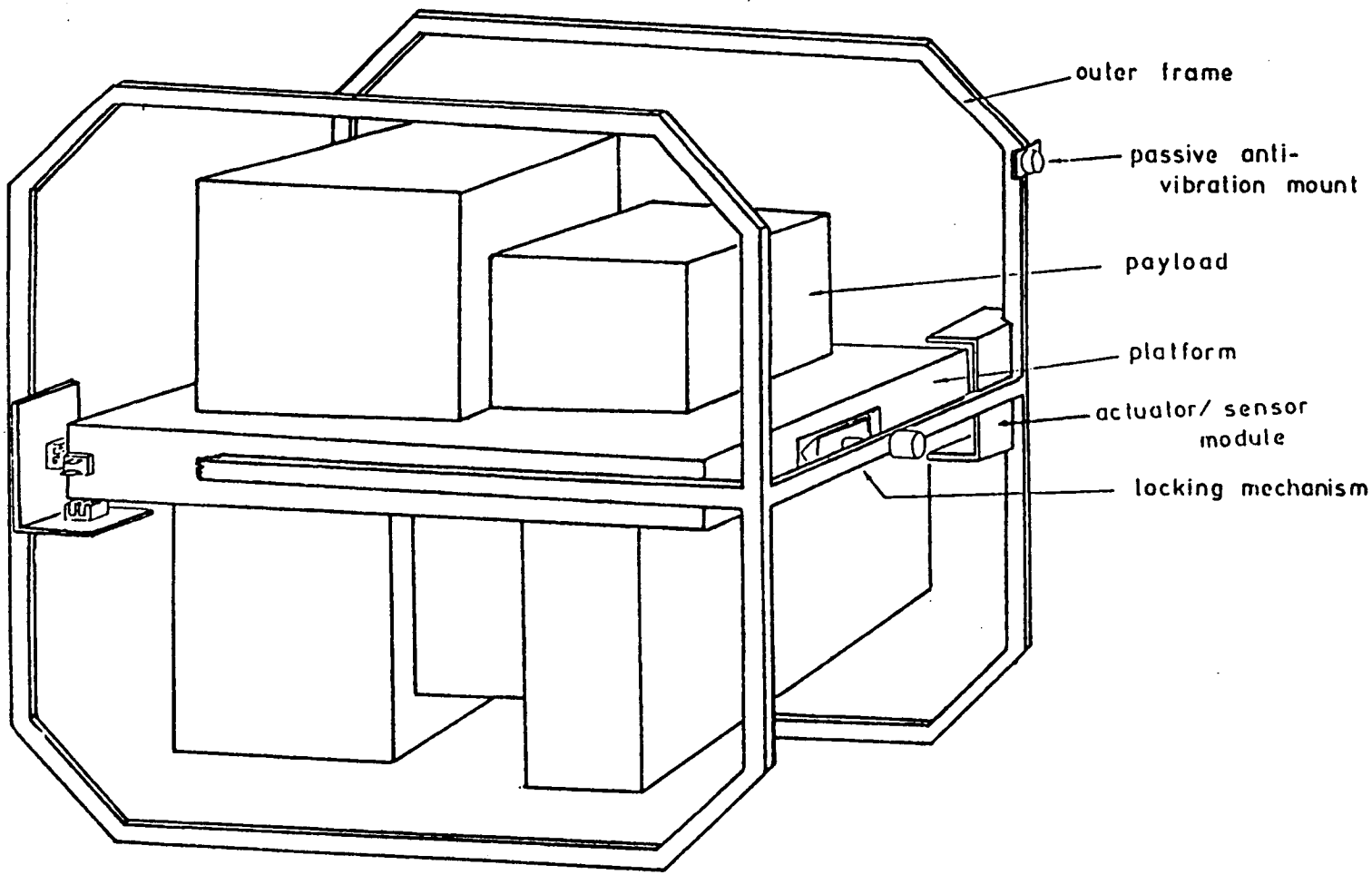

Fig.3 Structure of microgravity isolation mount.

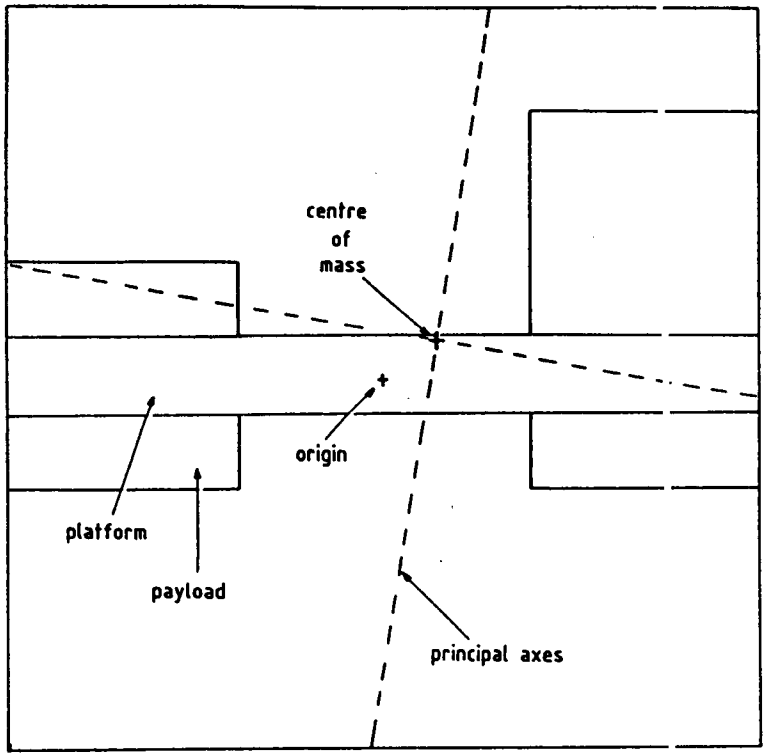

Fig.4 Platform/payload mass distribution typical case.

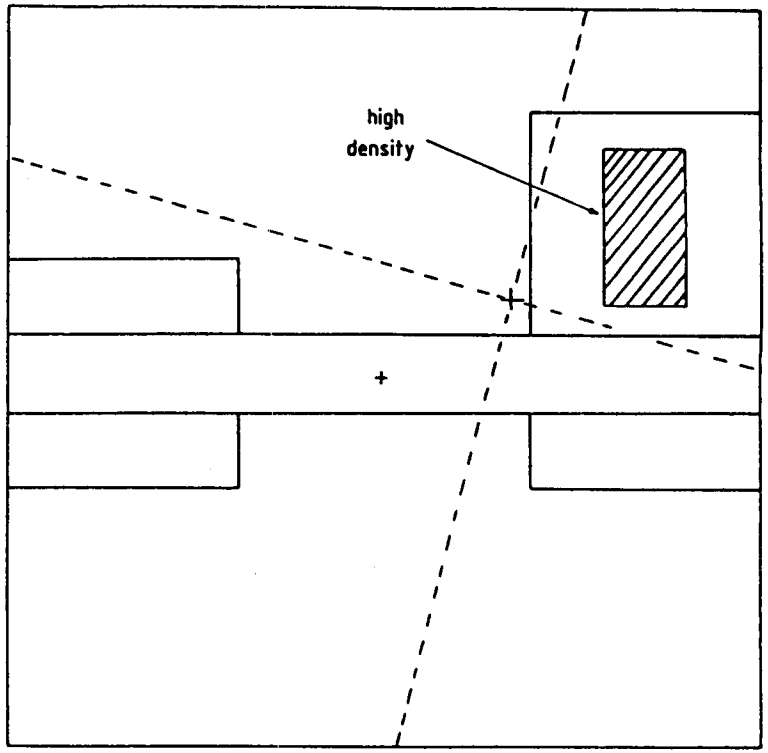

Fig.5 Platform/payload mass distribution asymmetric case.

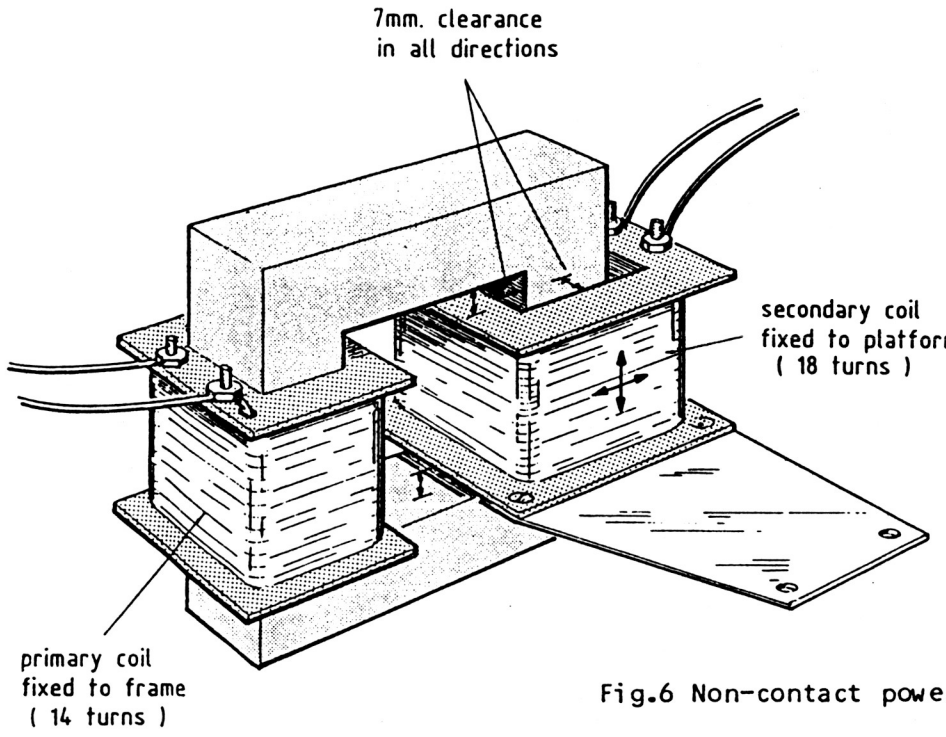

Fig.6 Non-contact power transformer.

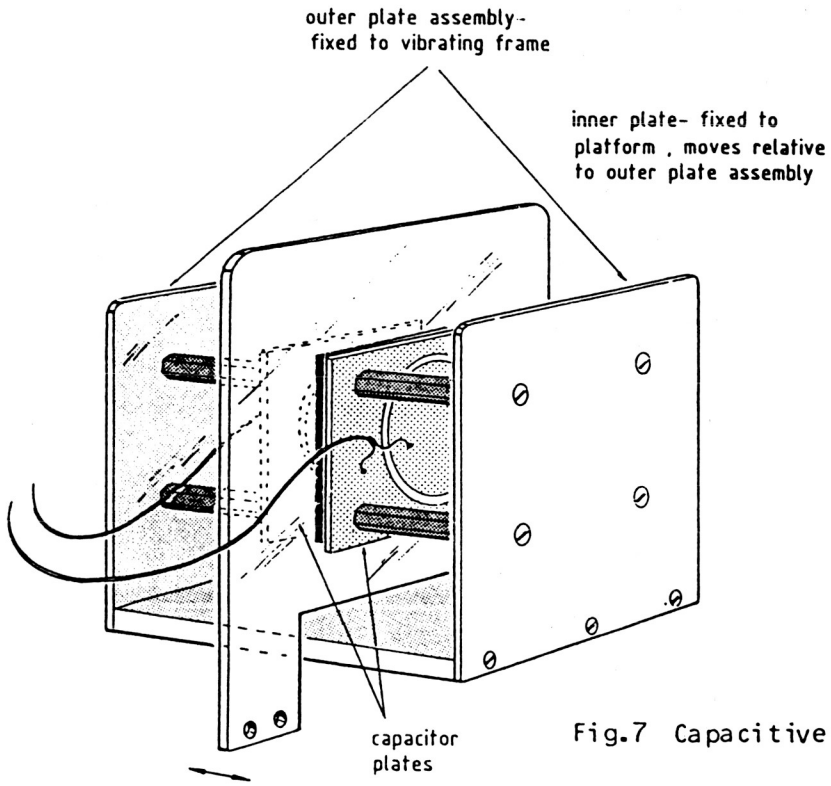

Fig.7 Capacitive position transducer.

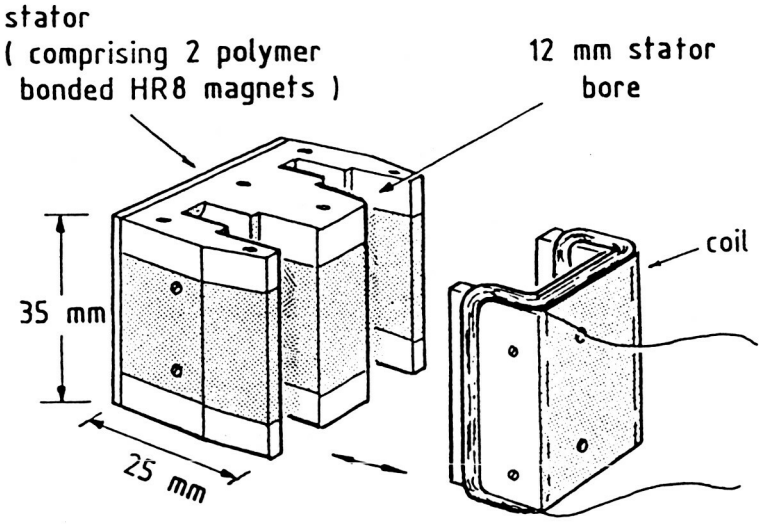

Fig.8 Actuator.

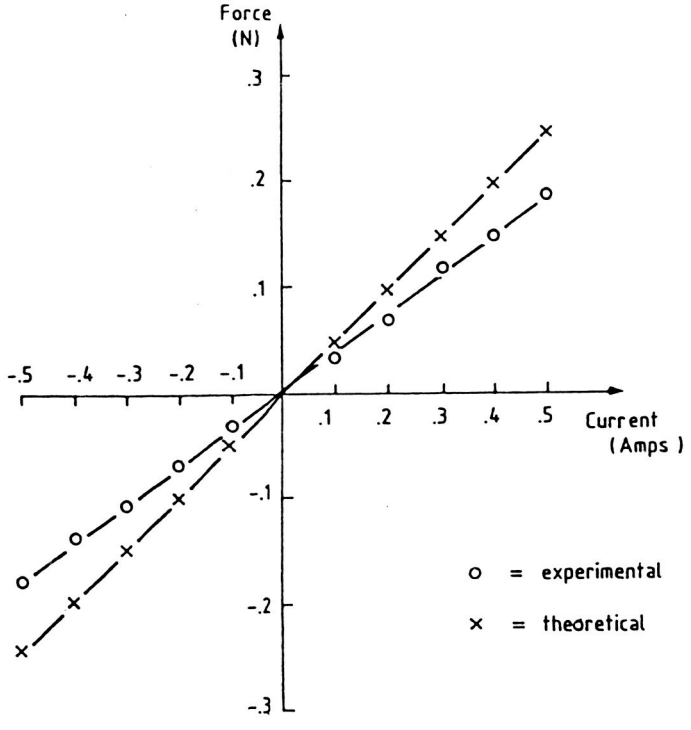

Fig.9 Measured force characteristic of actuator.

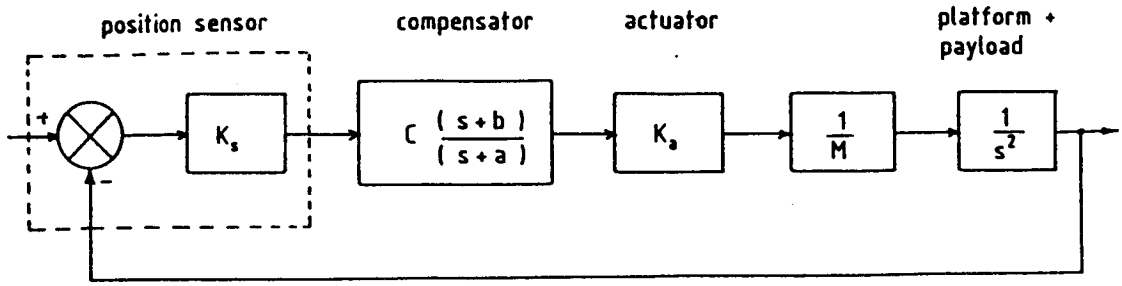

Fig.10 Block diagram of control loop.

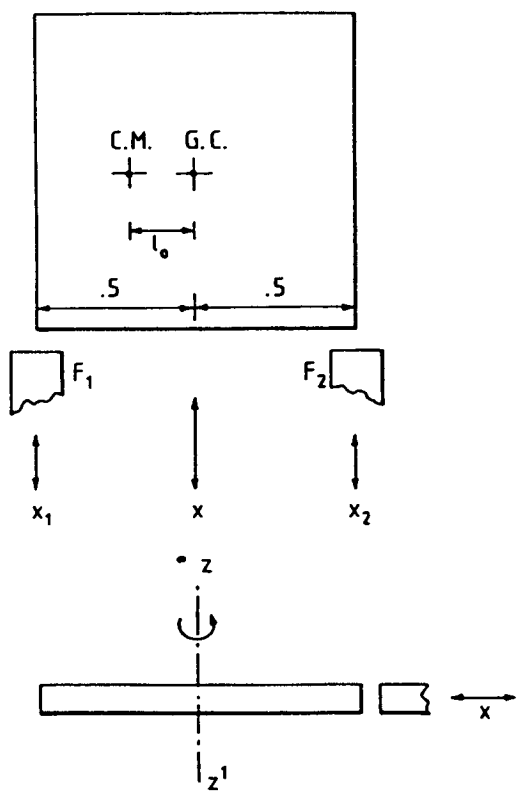

Fig.11 Two degree of freedom model.

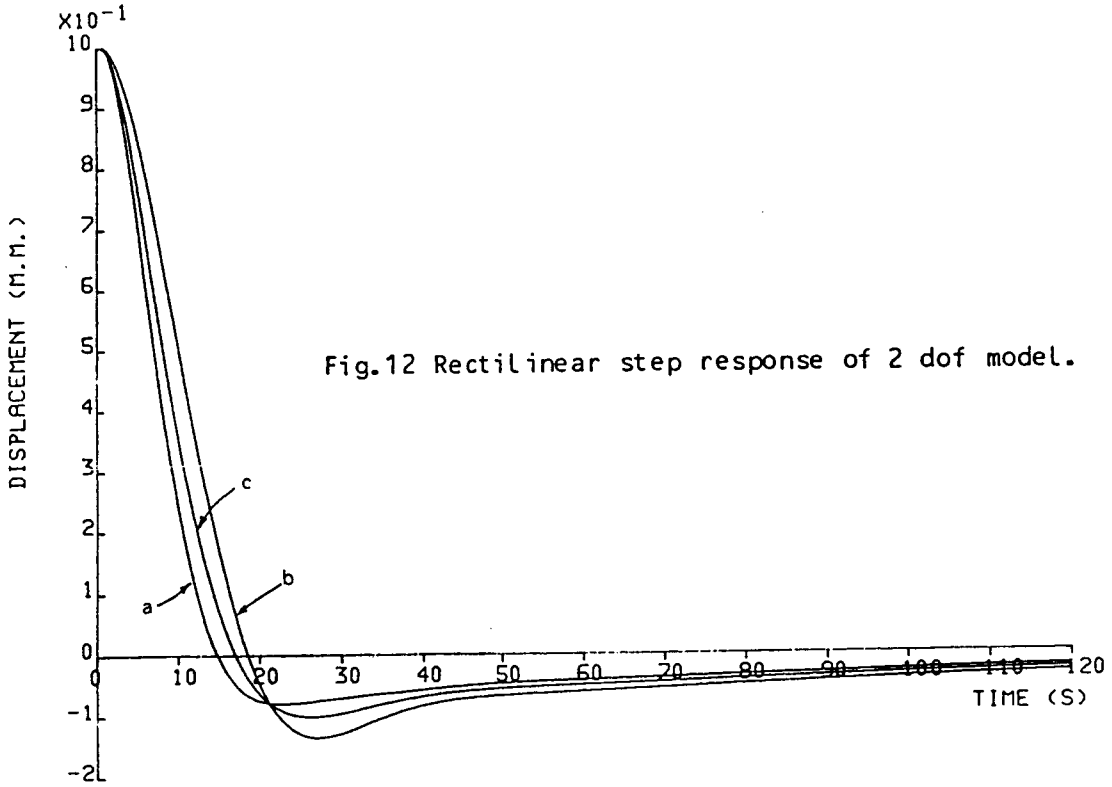

Fig.12 Rectilinear step response of 2 dof model.

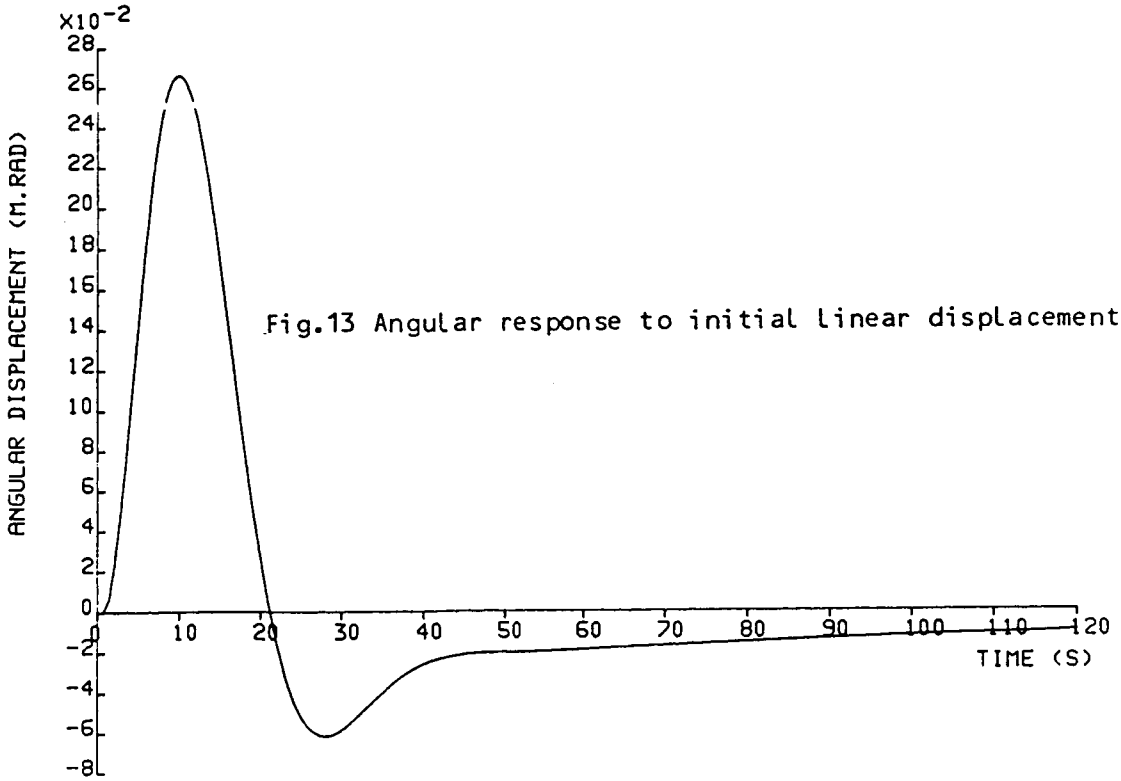

Fig.13 Angular response to initial linear displacement.

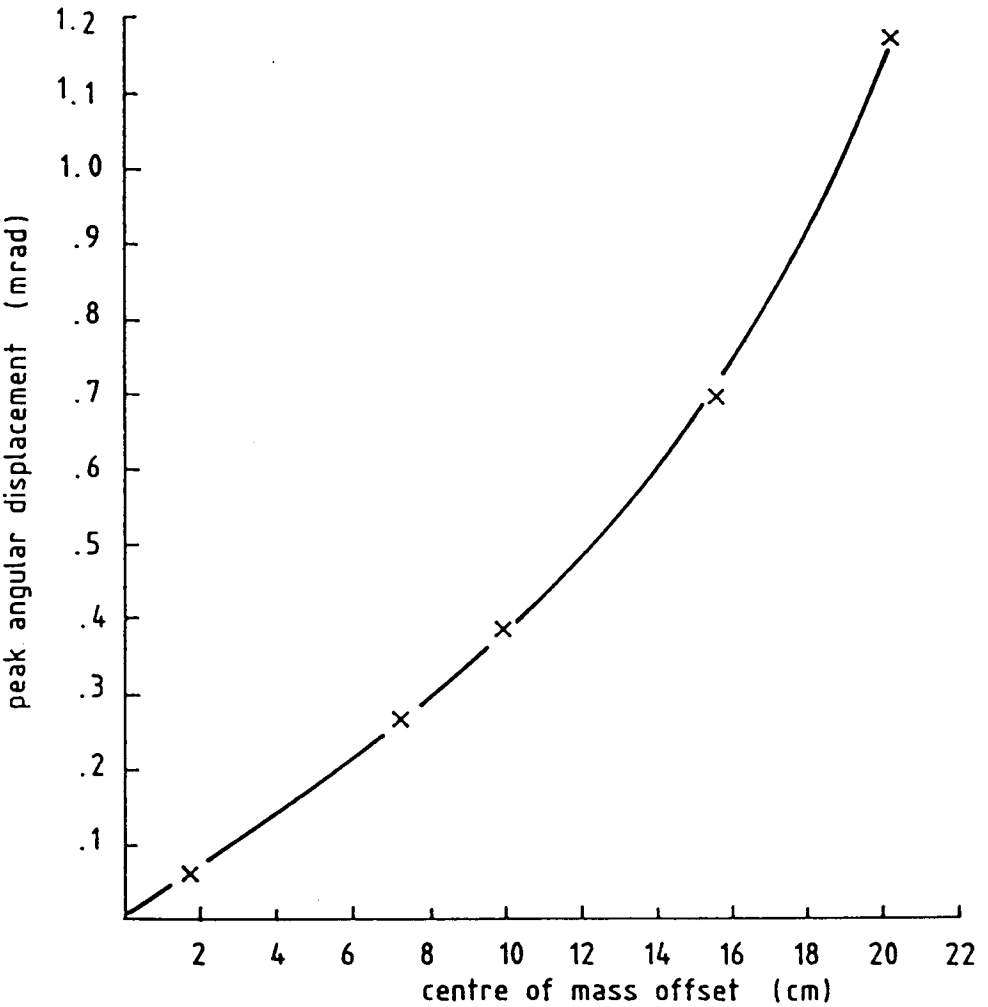

Fig.14 Variation of peak angle with centre of mass.

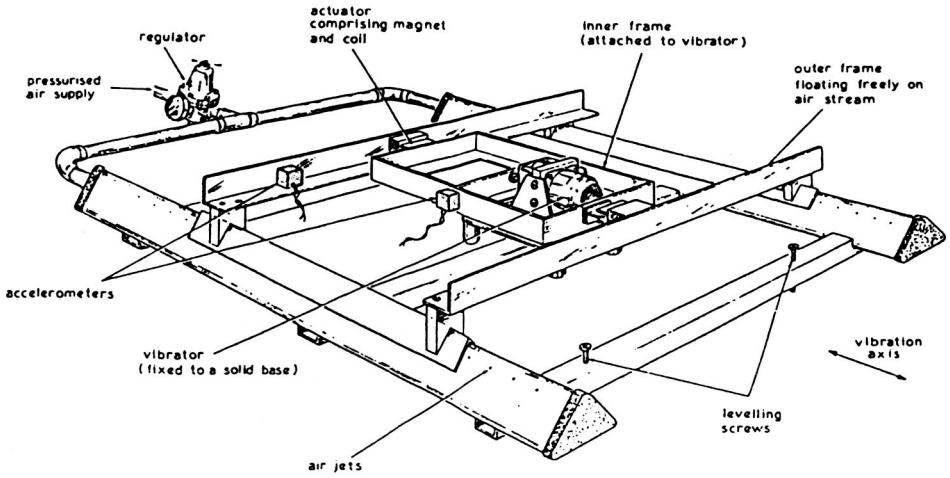

Fig.15 One degree of freedom test rig.

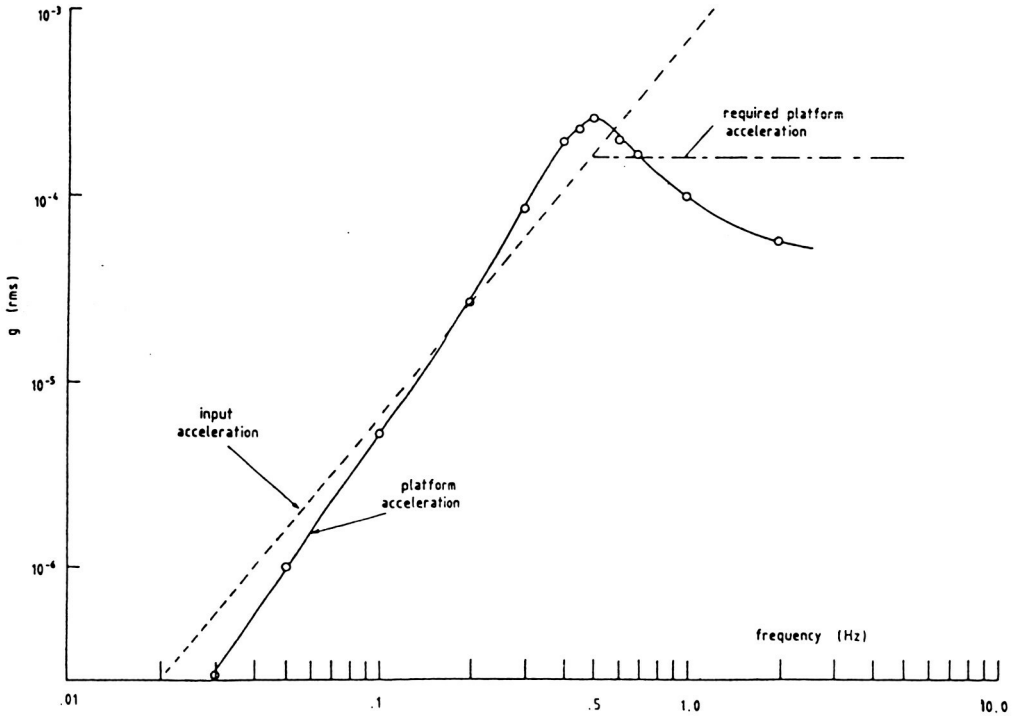

Fig.16 Measured results from 1 d.o.f. test rig.

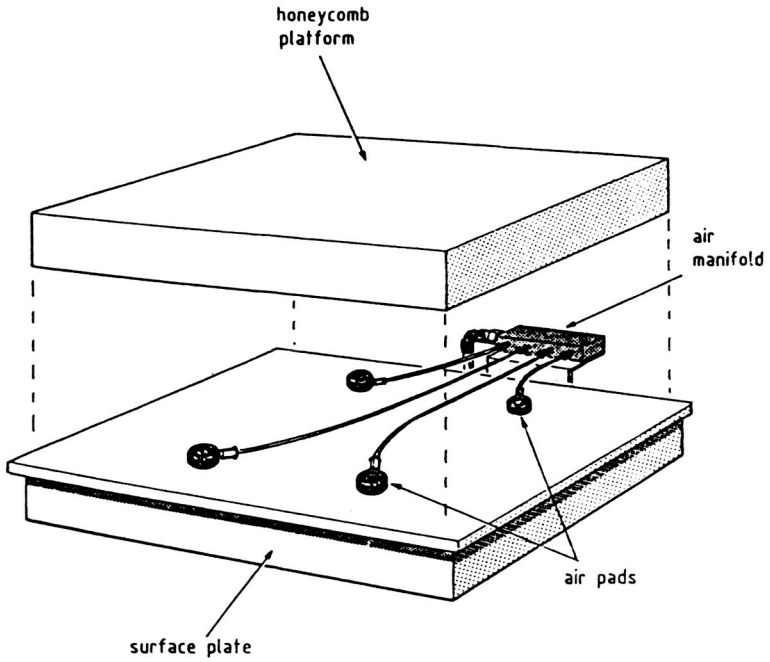

Fig.17 Three degree of freedom test rig.

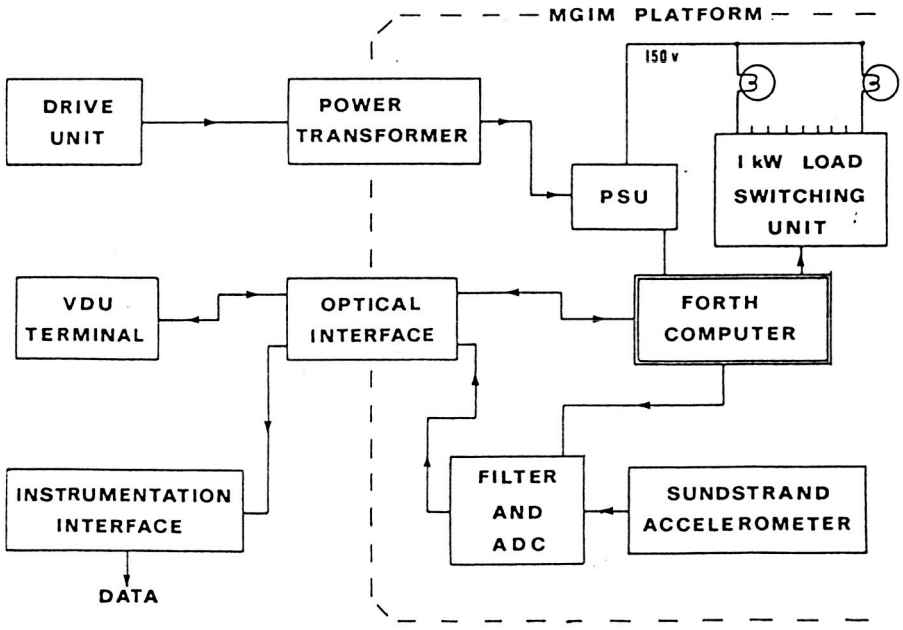

Fig.18 Instrumentation for 3 d.o.f. test rig.